Dynamic modeling of modular fuel cell for maximum power point tracking and torque ripple reduction in direct torque control of induction motor

Majid VALIZADEH*, Mohammad Reza FEYZI, Ebrahim BABAEI, Mehran SABAHI
Faculty of Electrical and Computer Engineering, University of Tabriz, Tabriz, Iran

Abstract: This paper presents a comprehensive dynamic model of a proton exchange membrane fuel cell (FC) based on the electrical empirical model. The presented model is useful for online control as well as having suitable accuracy. FC stacks produce a DC voltage with a ratio of 2:1 in output from no-load to full-load. In vehicles that are equipped with FCs, the output voltage of the FC is drastically changed because the power and torque of the vehicle change with the driving cycle. In order to improve the performance of the direct torque control of induction motors, the modular structure of a FC is proposed. This proposed structure guarantees the maximum power point tracking and torque ripple reduction. The validity of the proposed structure is satisfied by simulation results using MATLAB/Simulink software.

Key words: Fuel cell, dynamic modeling, modular structure, direct torque control, induction motor

1. Introduction

With the world facing the global warming problem related to fossil fuels, there is much attention to fuel cells (FCs) as a replacement energy source due to their high energy efficiency and being environmentally adaptive. FCs are electrochemical devices that convert chemical energy directly into electrical energy.

Among the different types of FCs, the proton exchange membrane FC (PEMFC) shows more advantages, such as the capability of working at low temperatures and having high-power density, fast response, and zero emissions. Hence, these types of FCs are suitable for use in portable power supplies and vehicles.

In a recent work, Palma [1] introduced a modular structure for a FC by dividing the stacks into 3 parts. However, the reason for this number of divisions was not discussed. Furthermore, he used a pure resistive load for the FC, which ignores the dynamic characteristic of FCs. In practice, the FC load can be an electrical motor, which differs from a pure resistive load. In this case, the dynamic behavior of the FC and motor characteristics should be taken into account.

In this paper, a new modular structure of a FC is proposed, which includes the dynamic characteristics of a FC and induction motor. In addition, it has the following advantages:

- Reduction of extra heating in underperforming sections of the stack,

- Shortening of the working time for weak cells,

- Generation a nearly constant output voltage.

---

*Correspondence: m-valizadeh@tabrizu.ac.ir

FC vehicles are a major category of new clean vehicles that have special characteristics and limitations. However, many of the existing papers did not include all of the above features, and as some of these features are related to others, neglecting a number of them causes a decrease in the dynamic model's accuracy. Some of the previous works focused on FC modeling without considering the characteristics of the load [2,3]. Some of the others used a static RL load rather than an electrical motor, such as [4]. This ignores the dynamic effect of the motor on the system's behavior, particularly when the system is operated at different speeds.

In this paper, a modular model of a FC is proposed. In this work, a variable speed induction motor is presented, where the direct torque control (DTC) method is used as a load. The dynamic equations of the induction motor and the drive system are also included in the model.

Many parameters of the FC, including the Nernst voltage, oxygen concentration, activation potential, water concentration, and resistance of the cell membrane, depend on the temperature of the FC. Therefore, in the proposed model, the variation of the FC temperature in the FC current is extracted and used to improve the accuracy of the model.

In this paper, first, the comprehensive dynamic model for the FC is presented, and then the DTC and related equations are introduced. After this, a new modular structure for the FC is proposed. Finally, the simulation results using MATLAB/Simulink software are given to prove the capability of the proposed model.

2. Review of FC modeling and DTC

The FCs used for portable applications should be small in size and have the ability to operate in ambient conditions. The most promising FC technologies for portable applications are air-breathing, direct methanol, and PEMFCs [5].

Direct methanol FC (DMFC) is a kind of polymer electrolyte membrane FC, which is directly fed with methanol instead of hydrogen. In comparison with the hydrogen PEMFC, although the DMFC has lower efficiency and power density, it has 3 times higher storable energy density [6].

A small DMFC is passively fed without external ancillaries such as pumps, blowers, and fans, which results in a very simple structure. It presents several advantages in terms of compactness, weight, scalability, durability, and maintenance [7].

In [8], a new dynamic model was established as a mathematical model for investigating the nonlinearity of a PEMFC. This model is based on physical laws, has clear significance in replicating the FC system, and can be easily used to set up different operational strategies.

From an empirical point of view, a formulated model was presented in [9] that enables simulation of the V-I curve (cell voltage versus current density) of both a FC and an electrolyzer under different conditions.

In [10], a purely electronic circuit model of a PEMFC was presented that can be utilized to design and analyze FC power systems using bipolar junction transistors and inductor-capacitor elements.

In [11], a simple and useful equivalent circuit based on a series connection of several Thévenin equivalent circuits was introduced. In this model, the output power of the stack is limited by the weakest cell. The state of a cell can be inferred from the voltage across its terminals, which is affected by parameters such as membrane humidity, air pressure, and fuel.

In [1], a modular model of a FC powered by a modular DC–DC converter was presented. In this model, the FC stack is divided into various sections, each powered by a DC–DC converter. This structure eliminates many of the stack disadvantages and increases the reliability of the FC operation.

The majority of studies have focused on the modeling, simulation, and optimization of a FC. FC models are complex and time-consuming; therefore, some of them are impossible for real-time emulation [12].

When the load changes fast, a suitable control is necessary. The best results are typically achieved using model-based control strategies.

In [13], a control-oriented PEMFC system model was presented in state space, which is suitable for the implementation of advanced control strategies, such as multivariable control with decoupling, actuator sensitivity analysis, or maximum efficiency tracking algorithms.

The conventional method for changing the output power of a FC is to change the pressure of the input gas. FC power controlling has been done with variable flowing air to the FCs [14].

The other method for controlling the output power of a FC is to control the cell's internal resistance. This might be accomplished by varying the membrane water content in a PEMFC or by varying the temperature in a solid oxide FC [15].

Various techniques are used for controlling squirrel cage induction motors. Among the different control methods, the DTC technique is the most common, relatively complete, and easily implementable method with a quick response. This technique is a combination of the field-oriented control (FOC) and direct self-control techniques. The DTC technique operates based on the measured motor voltage and current and is able to calculate the best switching state based on the measured values. This technique can be implemented with or without speed sensors, depending on the method used to estimate the stator flux [16].

Four different switching algorithms using hysteresis and nonhysteresis controllers were presented in [17]. In [18], a model predictive DTC was presented. It significantly reduces the switching losses and/or the harmonic distortions of the torque and stator currents in comparison with schemes such as DTC or pulse-width modulation (PWM). However, the computational burden is greatly increased due to the combinatorial explosion of the number of admissible switching sequences.

3. FC dynamic modeling

The actual cell potential decreases from its equilibrium potential due to irreversible losses. There are 3 types of irreversible losses: activation losses, ohmic losses, and concentration losses. At low current densities, the activation losses that reduce the oxygen reaction are almost entirely responsible for the potential drop of the cell. However, at high current densities, the concentration losses become more significant. The output voltage of a single cell is given by Eq. (1), according to the PEMFC output characteristics empirical equation [19]:

$$V_{FC} = E - V_{act} - V_{con} - V_{ohm}, \tag{1}$$

where E is the Nernst voltage (thermodynamic potential of the cell), which represents its reversible voltage; V_{act} is the activation overvoltage; V_{con} is the concentration overvoltage; and V_{ohm} is the ohmic overvoltage.

The Nernst voltage can be written as [20–22]:

$$E = \frac{\Delta G}{2F} + \frac{\Delta S}{2F}(T - T_{ref}) + \frac{RT}{2F}[ln(P_{H_2}) + \frac{1}{2}ln(P_{O_2})]. \tag{2}$$

The change of entropy is $\Delta S < 0$.

In some papers, such as [19,20], hydrogen pressure, P_{H2}, and oxygen pressure, P_{O2}, were supposed constant values, but these pressures are variable under different conditions. Choosing a constant value for these

pressures can reduce the model's accuracy. Since in our paper the cells are divided to categories according to their characteristics, the pressure of the input gases for each module may differ. The time constant, FC current, and number of cells in each module affect the oxygen and hydrogen pressure. The relationship between the molar flow of hydrogen and its partial pressure in the channel can be expressed as:

$$K_{H_2} \frac{q_{H_2}^{out}}{P_{H_2}}. \tag{3}$$

Based on the ideal gas law:

$$P \times V = n \times R \times T. \tag{4}$$

The partial pressure of each gas is proportional to the amount of gas in the cell, which is equal to the gas inlet flow rate minus the gas consumption and gas outlet flow rate [23].

$$\frac{dP_{H_2}}{dt} = \frac{RT}{V_a}(q_{H2}^{in} - q_{H2}^{out} - 2K_r I_{FC}) \tag{5}$$

$$\frac{dP_{O_2}}{dt} = \frac{RT}{V_C}(q_{O2}^{in} - q_{O2}^{out} - K_r I_{FC}) \tag{6}$$

$$K_{O_2} \frac{q_{O_2}^{out}}{P_{O_2}} \tag{7}$$

Here, q_{H2}^{in} and q_{O2}^{in} are the hydrogen and oxygen inlet flow rates, respectively. The constant K_r is defined by the relation between the rate of the reacting hydrogen and FC current. The hydrogen and oxygen pressures can be calculated by applying a Laplace transform; these partial pressures can be obtained in the s domain as [23,24]:

$$P_{H_2} = \frac{1/K_{H_2}}{1 + \tau_{H2}S}(q_{H2}^{in} - 2K_r I_{FC}), \tag{8}$$

$$P_{O_2} = \frac{1/K_{O_2}}{1 + \tau_{O2}S}(q_{O2}^{in} - K_r I_{FC}), \tag{9}$$

$$\tau_{H2} \frac{V_a}{K_{H_2}RT}, \tag{10}$$

$$\tau_{H2} \frac{V_C}{K_{O_2}RT}. \tag{11}$$

The activation losses of the PEMFC are caused by the sluggish kinetics of the reactions taking place on the active surface of the electrodes and can be computed by the following equation [21,25]:

$$V_{act} = -[\zeta_1 + \zeta_2 T + \zeta_3 T \times ln(C_{O_2}) + \zeta_4 T \times ln(I_{FC})]. \tag{12}$$

In some papers, the coefficients ζ_1, ζ_2, ζ_3, and ζ_4 are considered as constant values and in others they are considered as variable parameters depending on temperature, gas pressure, and FC current. If they are chosen as variable parameters, the stack voltage will not remarkably change because these coefficients are so small. This increases the time consumption and causes delays in calculating the proper voltage vector. As a result, the torque ripple will increase. Therefore, in this paper, constant values for these coefficients are considered.

There are different methods for calculating the ohmic voltage drop using experimental results and mathematics. The ohmic voltage drop is caused by the equivalent membrane impedance, RM, the contact resistances between the membrane and electrodes, and the electrodes and the bipolar plates, Rc [19]. In other words:

$$V_{ohm} = I_{FC} \times (R_m + R_c),\tag{13}$$

where

$$R_m = \frac{\rho_M \times l}{A},\tag{14}$$

$$\rho_M = \frac{181.6 \times [1 + 0.03 \times (\frac{I_{FC}}{A}) + 0.062 \times (\frac{T}{303})^2 \times (\frac{I_{FC}}{A})^{2.5}]}{[\psi - 0.634 - 3 \times (\frac{I_{FC}}{A})] \times \exp[4.18 \times (1 - \frac{303}{T})]}.\tag{15}$$

In the proposed dynamic model, the effect of concentration is also considered in the voltage drop calculation, which is different from some previous models. Concentration losses are caused by mass transportation, which, in turn, affect the concentration of the hydrogen and oxygen at a high current density. This term is ignored in some models, perhaps because it is not desirable to operate the stack in regions where concentration losses are high (efficiency is low). However, if the stack operates in high current applications, such as driving electric motors with heavy loads, this term should be included. The concentration voltage drop can be expressed as:

$$V_{con} = -\frac{RT}{2F} ln(1 - \frac{J}{J_{\max}}).\tag{16}$$

Some papers, such as [22,25], state the concentration voltage as below:

$$V_{con} = -B \times ln(1 - \frac{J}{J_{\max}}),\tag{17}$$

where B is a parametric coefficient, which depends on the cell and its operating state. In this paper, the FC current is used to feed a motor. The required motor current will be changed under different conditions and so the FC current must be changed. Therefore, the FC temperature will be changed. Papers that chose B as a constant coefficient in their modeling have less accuracy, especially at a high current density. Therefore, we use Eq. (16) for the concentration voltage.

There is a charge double layer in the PEMFC that has been analyzed on the surface of the FC cathode. This part can be modeled by a capacitor. The equivalent circuit of the PEMFC is shown in Figure 1, where R_a is the equivalent resistance, which includes the activation equivalent resistance, R_{act}, and the concentration equivalent resistance, R_{con}. The equivalent capacitance, C, can effectively smooth the voltage drop. The main characteristics of the PEMFC dynamic behavior can be considered as a function of the charge double layer.

One of the most important parameters that affect the FC output voltage is the FC temperature. The Nernst voltage, oxygen concentration, activation over potential, water concentration, and resistance of the cell membrane depend on the temperature.

Figure 1. Equivalent circuit model of the PEMFC.

The FC temperature was assumed to be constant in some previous works [19,23,26]. However, the FC temperature is an important effector parameter on its output dynamic behavior. The FC temperature variation can be expressed as [5]:

$$T = T_{ic}I_{FC} + T_{rt}e^{(\frac{I_{FC}}{T_{it}}t)}, \tag{18}$$

where T_{ic}, T_{rt}, and T_{it} are constant parameters for the FC temperature and I_{FC} is the FC current.

A block diagram of the proposed PEMFC dynamic model in MATLAB/Simulink is illustrated in Figure 2. This dynamic modeling is more comprehensive than that in [19] because:

Figure 2. PEMFC dynamic modeling in MATLAB/Simulink.

a) The pressure of the hydrogen and oxygen can change dynamically, but it was ignored in [19].

b) In [19], the temperature of the FC was considered as constant, but in the proposed model, it is considered as a function of FC current.

c) The FC current is a dependent variable that depends on the voltage and load of the FC, but in [19], the FC current was considered as an independent variable.

d) The presented model in [19] was an open-loop model, but this paper presents a closed-loop model that uses the output current of the FC for calculation of the parameters of voltage drop.

4. DTC of the induction motor fed from the FC

The induction machine equations in terms of the space vectors in a stator reference frame are as follows:

$$\bar{v}_s = R_s \bar{i}_s + \frac{d\bar{\psi}_s}{dt}, \tag{19}$$

$$0 = R_r \bar{i}_r + \frac{d\bar{\psi}_r}{dt} - j\omega_r \bar{\psi}_r, \tag{20}$$

where ω_r is the rotor angular speed in the electrical radians and $\bar{v}_s$ is the stator voltage space vector. $\bar{i}_s$ and $\bar{i}_r$ are the stator and rotor current space vectors, and R_s and R_r are the stator and rotor resistances, respectively. $\bar{\psi}_s$ and $\bar{\psi}_r$ are the stator and rotor flux linkages, respectively, which are given as:

$$\bar{\psi}_s = L_s \bar{i}_s + L_m \bar{i}_r, \tag{21}$$

$$\bar{\psi}_r = L_r \bar{i}_r + L_m \bar{i}_s, \tag{22}$$

where L_s and L_r are the stator and rotor self-inductances, respectively.

Unlike in FOC, the DTC scheme offers a simple control structure. In the DTC scheme, the torque and flux can be separately controlled using hysteresis comparators, as shown in Figure 3. The FC voltage is controlled by the amount of speed and torque errors, which will be explained in Section 5. The stator flux can be directly calculated from the stator voltage equations in the stator reference frame, as follows:

$$\psi_{sd} = \int (u_{sd} - R_S i_{sd}) dt, \tag{23}$$

$$\psi_{sq} = \int (u_{sq} - R_S i_{sq}) dt, \tag{24}$$

$$|\bar{\psi}_s| = \sqrt{\psi_{sd}^2 + \psi_{sq}^2}. \tag{25}$$

The proper switching pattern of the inverter is achieved using the current and voltage of the phases, as well as the reference speed and calculation of the required stator flux and torque. Since the motor input voltage contributes to both the flux and the required torque, selecting a proper switching pattern for an inverter is very important. In many of the non-PWM switching patterns used in the DTC technique, the flux and torque are independently controlled using the hysteresis controllers.

Figure 3. Schematic diagram of the proposed DTC for the IM motor fed from the FC.

In the proposed technique, the difference between the stator flux and its reference value (flux error) and the difference between the motor torque and its reference value (torque error) are controlled by a hysteresis cycle with a predefined threshold. The level of these errors dictates the inverter switching pattern.

The torque and flux of the motor can be calculated using 2 current sensors and considering the switches' states, as follows:

$$u_{sd} = \frac{2}{3}V_{FC}(S_A - \frac{S_B + S_C}{2}), \tag{26}$$

$$u_{sq} = \frac{1}{\sqrt{3}}V_{FC}(S_B - S_C), \tag{27}$$

$$i_s = i_{sd} + ji_{sq} = \frac{2}{3}(i_{SA} + ai_{SB} + a^2i_{SC}), \tag{28}$$

Here $i_{SA} + i_{SB} + i_{SC} = 0$, so the following can be concluded:

$$i_{sd} = i_{SA}, \tag{29}$$

$$i_{sq} = \frac{i_{SA} + 2i_{SB}}{\sqrt{3}}, \tag{30}$$

$$T_e = \frac{3}{2}P(\psi_{sd}i_{sq} - \psi_{sq}i_{sd}). \tag{31}$$

The lookup table is given in Table 1, which is used for choosing the best voltage vector in each mode. In each section, different voltage vectors with different characteristics can be chosen. The better voltage vector can

be selected according to the situation of the flux and operating point. To reduce the switching frequency, the voltage vector is selected in such a manner that the variation of the switches' state is minimized.

Table 1. Lookup table for switching patterns.

$d\psi_s$	dT_e	S1	S2	S3	S4	S5	S6
-1	-1	$\bar{u}_2$	$\bar{u}_3$	$\bar{u}_4$	$\bar{u}_5$	$\bar{u}_6$	$\bar{u}_1$
-1	0	$\bar{u}_7$	$\bar{u}_0$	$\bar{u}_7$	$\bar{u}_0$	$\bar{u}_7$	$\bar{u}_0$
-1	1	$\bar{u}_6$	$\bar{u}_1$	$\bar{u}_2$	$\bar{u}_3$	$\bar{u}_4$	$\bar{u}_5$
1	-1	$\bar{u}_3$	$\bar{u}_4$	$\bar{u}_5$	$\bar{u}_6$	$\bar{u}_1$	$\bar{u}_2$
1	0	$\bar{u}_0$	$\bar{u}_7$	$\bar{u}_0$	$\bar{u}_7$	$\bar{u}_0$	$\bar{u}_7$
1	1	$\bar{u}_5$	$\bar{u}_6$	$\bar{u}_1$	$\bar{u}_2$	$\bar{u}_3$	$\bar{u}_4$

5. Proposed modular structure of the FC

The output voltage of each cell is very small, so to generate the required voltage for the motor, many cells must be connected in series. In theory, due to the input manifold, the fuel pressure on each cell is considered constant, but in real systems, it may drop due to water condensation or other obstructions. The cells that receive lower pressure will produce less voltage.

The value of membrane humidity may vary between different cells depending on the heat distribution within the FC. Cells with a drier membrane will produce less voltage than cells with a more moisturized membrane.

Different cells have different V-I and P-I characteristics. In each stack, the maximum current of the stack is limited to the weakest cell current. Therefore, the obtained power from the stack is decreased. If the load current exceeds the maximum current of the weakest cell for a long period of time, the stack will be overheated due to the additional internal losses. Hence, the cells that are not performing properly may be out of service or be disconnected by the operator.

To optimize the operation of the stack, each individual cell's current flow should be controlled independently. However, in practice, this ideal situation rarely occurs; instead, the division of the stack into 5–10 cell sections is more practical.

In the first step, cells are categorized based on their maximum power (P_{max}) and current (I_{pmax}). The cells with larger P_{max} and I_{pmax} are located in the lower modules of the series' construction. The number of cells in each module is determined by the power of the motor, as well as the required speed and torque range.

The motor is started at no load with a minimum acceptable number of modules. Next, the instantaneous torque and speed of the motor are monitored continuously. Any change in the reference torque or speed results in a transient condition; this is monitored by the control system and then the required number of modules in the stack is calculated. Otherwise, without a change in reference values, the number of modules remains constant. The value of k depends on the motor power and other driving conditions. The control system may lose its stability in the case of an inadequate module number so that the motor cannot trace the reference speed and torque.

In steady-state condition, the operator can select either maximum power point tracking (MPPT) or torque ripple reduction, depending on operating conditions. If the torque ripple reduction is selected as the first priority, the average value of 10 sampled torque errors is compared with an acceptable level of error. If the torque ripple exceeds the determined value, the number of modules should be decreased. In the DTC method, the torque ripple depends on the value of the voltage vector, which is from the FC. Therefore, the torque ripple

can be decreased by adjusting the modular FC. The torque slope can be calculated as follows:

$$\bar{u}_s = \bar{u}_k = \frac{2}{3}V_{FC}\left[j(k-1)\frac{\pi}{3}\right] \quad k = 1, 2, ..., 6, \tag{32}$$

$$S_r = -T_e(\frac{R_s}{\sigma L_s} + \frac{R_r}{\sigma L_r}) + (\frac{3}{2})(\frac{P}{2})\frac{L_m}{\sigma L_s L_r}Im([u_s.\lambda_r^*] - j\omega_m[\lambda_s.\lambda_r^*]), \tag{33}$$

where S_r is torque increment slope. This slope depends on the motor speed, motor torque, and voltage vector. Eq. (33) has 3 parts, which can be written as:

$$S_r = S_{ra} + S_{rb} + S_{rc}, \tag{34}$$

$$S_{ra} = -T_e(\frac{R_s}{\sigma L_s} + \frac{R_r}{\sigma L_r}), \tag{35}$$

$$S_{rb} = (\frac{3}{2})(\frac{P}{2})\frac{L_m}{\sigma L_s L_r}|u_s||\lambda_r|\sin(\theta_v - \theta_r), \tag{36}$$

$$S_{rc} = -(\frac{3}{2})(\frac{P}{2})\frac{L_m}{\sigma L_s L_r}\omega_m|\lambda_s||\lambda_r|\cos(\theta_s - \theta_r). \tag{37}$$

Therefore, the voltage amplitude and vector angle must be determined to satisfy the desired torque increment slope. The proper voltage vector angle can be obtained from a lookup table. Some papers have focused on improvement of the lookup table. In this paper, a modular algorithm is used to control the amplitude of the voltage vector, which determines the FC output voltage. To decrease the torque when the torque error reaches the upper level of the hysteresis band, the zero-voltage vectors must be applied, which leads to a decrease in the torque ripple, switching frequency, and switching losses. Therefore, the slope of the torque reduction becomes:

$$S_f = -T_e(\frac{R_s}{\sigma L_s} + \frac{R_r}{\sigma L_r}) - (\frac{3}{2})(\frac{P}{2})\frac{L_m}{\sigma L_s L_r}\omega_m|\lambda_s||\lambda_r|\cos(\theta_s - \theta_r). \tag{38}$$

As mentioned earlier, the output power of a FC drops when its current exceeds its critical point; this point is also called the maximum power point. In the proposed modular algorithm, the voltage of the last module in the stack acts as a criterion to determine the number of modules. If the output voltage of this module becomes less than V_{pmax}, the module is operating beyond its critical point and, therefore, the number of modules must be increased in order to obtain the maximum power from the cells. In addition, this will result in the elimination of excess thermal stress on the cells, caused by exceeding the current from I_{pmax}. Therefore, the proposed algorithm guarantees the torque ripple reduction and MPPT. A block diagram of the proposed modular structure of the FC used in a DTC-controlled induction motor drive is shown in Figure 4.

6. Simulations and discussion

In this section, the simulation results of the proposed dynamic model for the FC and modular structure are carried out. Next, the DTC performances in both cases, when the motor is fed from the FC and from a constant DC voltage source, such as an ideal battery, are compared. The parameter's values of the FC and induction motor are listed in Table 2.
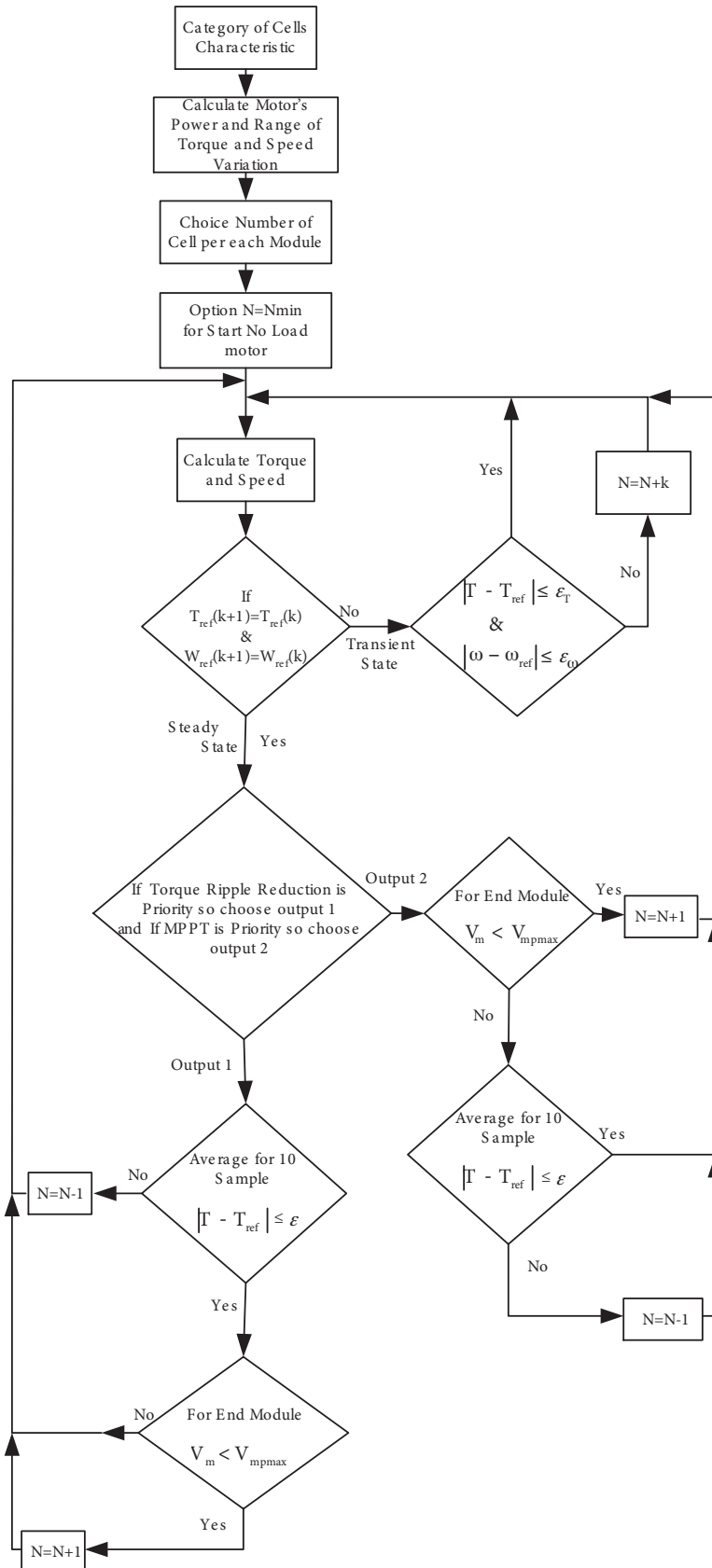
Figure 4. Diagram of the proposed modular structure for the FC.

Table 2. Symbol and parameter values.

Parameter	Value	Parameter	Value
ΔG	237180 J mol^{-1}	l	51 μm
F	96486.7 C mol^{-1}	T_{ic}	8.5
ΔS	−163.15 mol K	T_{rt}	11.2
T_{ref}	298.15 K	T_{it}	1500
R	8.314 J mol^{-1} K^{-1}	R_s	1.115 Ω
K_{H2}	3.63×10^{-5} K mol atm^{-1} s^{-1}	R_r	1.083 Ω
τ_{H2}	0.3096 s	L_s	0.005974 H
ζ_1	−0.9514	L_r	0.005974 H
ζ_2	0.00312	L_m	0.2037 H
ζ_3	7.4×10^{-5}	Motor power	5 HP
ζ_4	-1.87×10^{-4}	V$_{LL}$	460 V
R_c	0.0003 Ω	Frequency	60 Hz
ψ	20	Nominal speed	1750 rpm

The membrane resistivity from Eq. (15) is given in Figure 5, which shows the effect of the increment of current and temperature on membrane resistivity. This simulation is carried out by setting $\psi = 20$. One of the problems that increases the nonlinearity and complexity of the FC characteristic is the dependence of the FC's temperature on its current. A current increment causes a temperature increment, but temperature and current have an inverse effect on membrane resistivity.
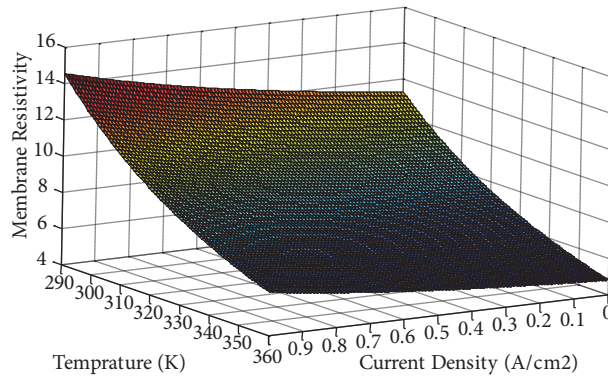
Figure 5. Membrane resistivity according to the current density and temperature.

In a stack, cells have different characteristics, like the V-I and P-I curves, and different conditions, such as different temperatures, pressures, and moisture levels. The V-I and P-I curves of a cell are simulated when the temperature is changed by 30°. Figure 6 shows the results of this simulation. It is noticeable that when the temperature changes, P_{max} and I_{pmax} change consequently. This simulation shows that in a stack with many cells, cells have different conditions, such as temperature. Therefore, each cell produces a different voltage from the others, so P_{max} and I_{pmax} will be different. In this condition, the maximum current of the stack is limited to the I_{pmax} of the cell that has the worst conditions. Therefore, the maximum power is limited. The modular structure proposed in this paper categorizes the cells in such a way that this problem can be solved.

To confirm the validity of the proposed dynamic modeling and modular algorithm for the DTC, simulations are carried out in 2 modes. In the first mode, the induction motor is fed from the battery, and in the second, it is fed from a modular FC. Two hysteresis controllers are used to control the flux and torque, 2-level

for the flux and 3-level for the torque. With a large hysteresis band width, the torque ripple is increased, but with a very small one, the switching frequency and switching losses are increased. In this paper, the band widths are chosen according to the motor parameters.
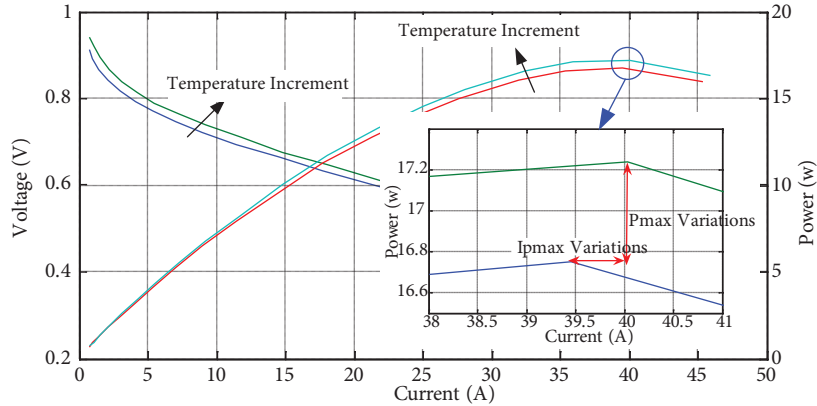

Figure 6. V-I and P-I curve of a cell when the temperature is changed by $30°$.

To understand the ability of the proposed modular algorithm, the DTC is carried out with a battery as a constant DC source and then similar conditions are applied to the modular FC. The induction motor is initiated at no-load with a 300-rpm speed command. The initial current of the motor has a large magnitude for a short duration. If the voltage vectors are applied at the beginning of the motor starting, the motor current increases drastically because the flux of the motor is smaller than the proper value. One of the phase currents is shown in Figure 7. The nominal torque is applied at t = 0.7 s, so the current increases at this moment. The stator current is sinusoidal, while it has harmonics.
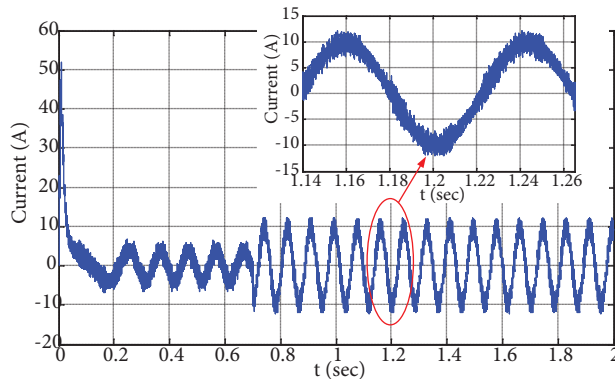
Figure 7. Stator current of the DTC IM fed from the battery.

The simulation results of motor speed and motor torque when the motor is fed from the battery are shown in Figures 8 and 9, respectively. The speed reference increases, such as a ramp function, in which its slope can be optimized according to the motor parameters and operating point. If a large amount is chosen for the reference speed slope, the amount of torque increment during the speed variation will be large. Therefore, the motor will overload. This can be explained as:

$$T_e = T_l + J_m \frac{d\omega_m}{dt}.$$ (39)

329

When the motor speed reaches 300 rpm, the current decreases and the motor torque returns to 0. When a nominal torque is applied to the motor, the motor speed falls about 18 rpm, and then after a short time, less than 0.06 s, the motor speed returns to the previous speed. The motor has good speed regulation when the load torque changes. The DTC has a fast dynamic response, so when a nominal torque is applied to the motor, the motor torque reaches the nominal value quickly. The torque ripple is about 6.5%, which is large. As mentioned above, this is one of the intrinsic problems of the DTC. The goal of this paper is the comparison of the modular FC for the DTC and the classical battery-fed DTC. Using additional methods, which can be found in previous papers, can improve the ability of the proposed structure, but on other hand, they lead to DTC complexity.
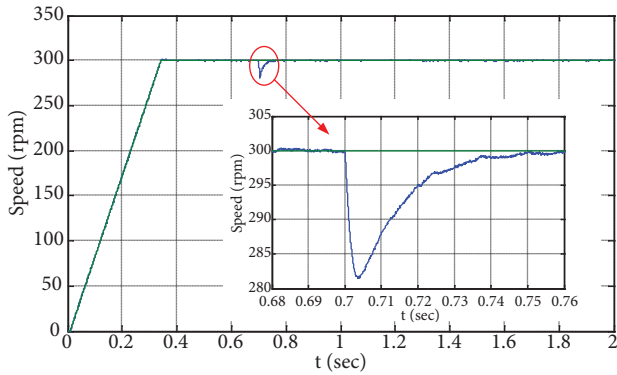
Figure 8. Motor speed in the DTC IM fed from the battery.
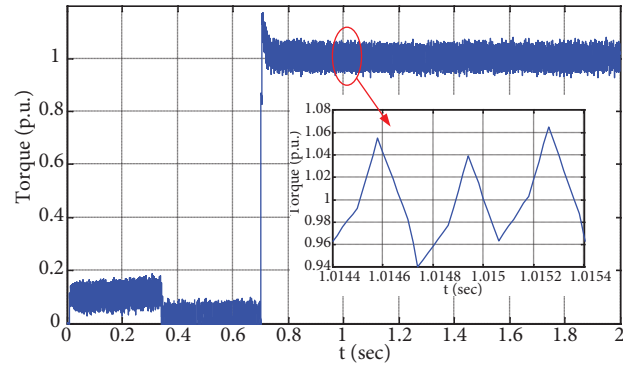
Figure 9. Motor torque in the DTC IM fed from the battery.

The same conditions apply to the induction motor, fed from the modular FC. The stator current, motor speed, and motor torque are shown in Figures 10, 11, and 12, respectively. The starting current is reduced by approximately 66%. Moreover, the stator current is sinusoidal and it has fewer harmonics than the battery-fed DTC induction motor. Therefore, the efficiency of the drive system increases. At the starting moment, the induction motor, which is fed from the FC, has a small delay of about 0.07 s. This delay is related to the FC start-up calculations. When a nominal torque is applied to the motor, the motor speed falls as much as the
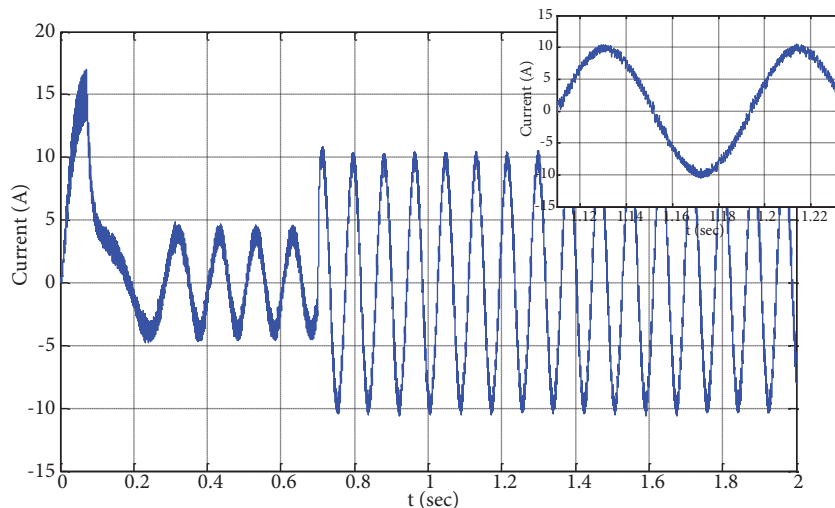

Figure 10. Stator current of the DTC IM fed from the FC.

battery-fed motor, but the time needed to return to its previous speed is 0.1 s. The speed regulation is as suitable as that of the battery-fed motor. Important improvement takes place in motor torque. The torque ripple is reduced to 2.5%, which is less than in the previous state.
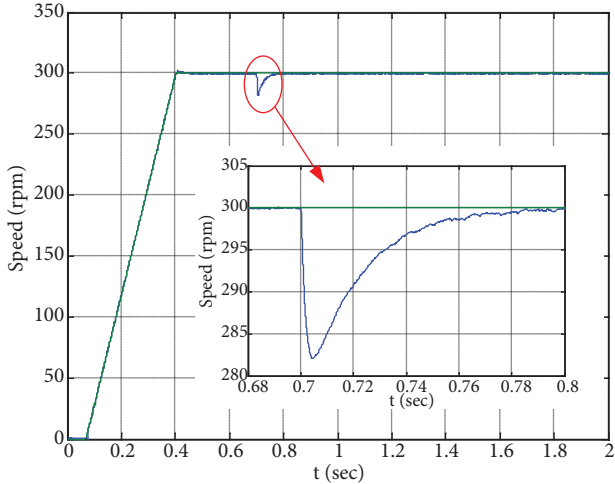

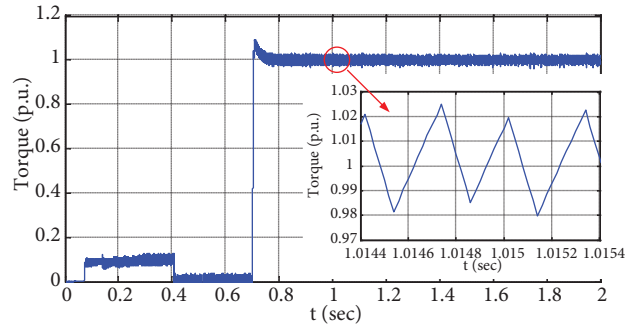**Figure 11.** Motor speed in the DTC IM fed from the FC.

Figure 12. Motor torque in the DTC IM fed from the FC.

If the flux proportional-integral (PI)ğ ğcontroller is designed to decrease the rise time of the flux response, the motor starting current will decrease, but the overshoot of flux response and probability of instability will increase. The best values for PI controller parameters are selected when the response of the flux is critical damping.

The stator flux trajectory in the d-q surface shows the transient-state and steady-state operation characteristics. During the initial build up, if the flux trajectory is along the radial path, it builds up quite fast [27]. If the components of the flux have a 90° phase difference and equal magnitude, the d-q flux curve is circular. A thin circle shows little flux ripple around the reference flux. Therefore, the quality of the circular flux route demonstrates the steady-state performance of the DTC [28].

In these simulations, the nominal flux is 0.8 Wb. During start-up, the control system increases the flux d component, while the q component is still held at 0. This strategy improves the transient characteristic of the DTC. The circular curve of the flux in the d-q plate is shown in Figure 13. The flux has little ripple around the nominal value, and the authors intend to reduce that in future works.

In the steady state, if the voltage vectors are decreased, the gradient of torque and flux variations will be small, so with the same time sampling and switching frequency, the torque ripple will be reduced. The modular FC not only reduces torque ripple but also increases the efficiency of the DTC because the harmonics of the stator current are reduced.

Therefore, for FC vehicles, if this modular algorithm is used, the distance that the vehicle can drive with one charge will be increased because the torque ripple and harmonics of the stator current, which cause more losses, are decreased and maximum power can be obtained from the FC.

One of the most important subjects in electrical vehicles is fast dynamic response. This paper uses a modular FC for the DC source. Therefore, it has more calculations in the DTC of the induction motor. The simulation results when a nominal torque is applied to the motor are shown in Figure 14. This response is quicker, but it needs about 0.005 s to reach the nominal torque, which is 0.002 s more than the battery-fed

motor under the same conditions. In order to increase the dynamic response speed, when the reference torque has large variation, the modular structure can stop the torque ripple minimization. Next, it increases the number of modules and selects a voltage vector to produce the largest torque component. When the torque reaches the proper value, the modular structure returns to the torque ripple minimization. Therefore, torque ripple increases only during the transient state, which is a very short time. The result of this strategy is shown in Figure 15. This improvement causes a faster dynamic response of about 20%.
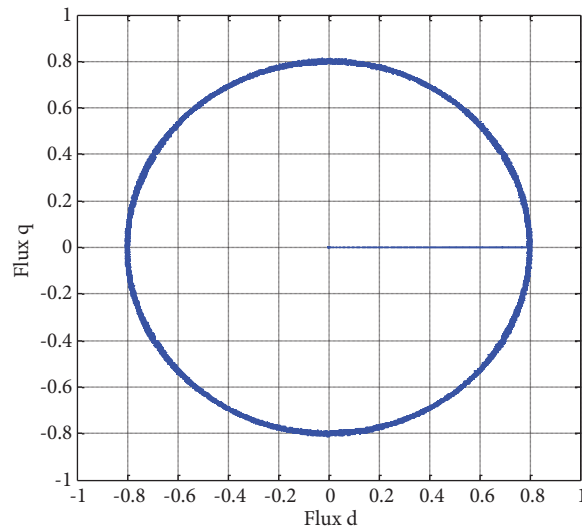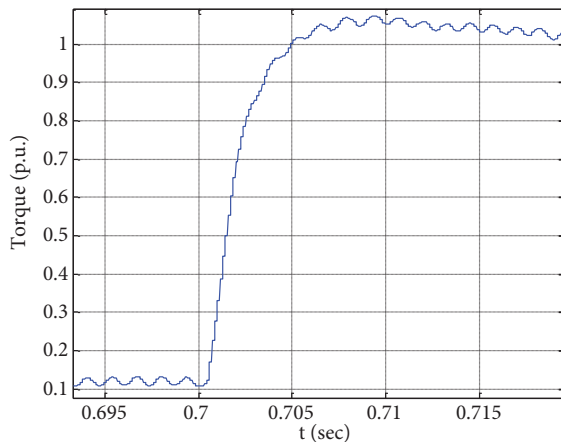

Figure 13. Circular flux curve.

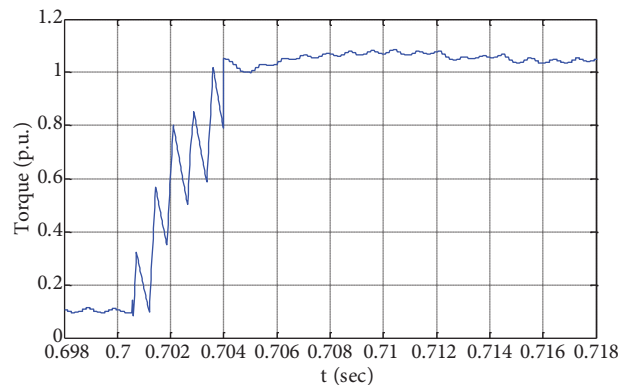**Figure 14.** Dynamic response of the DTC fed from the modular FC.

Figure 15. Dynamic response of the DTC fed from the improved modular FC.

7. Conclusion

A dynamic model for a PEMFC was proposed to take the dynamic effect of the variety of hydrogen and oxygen pressure changes into account during the operating conditions of a FC. In addition, a temperature change caused by the FC current was taken into account. This enables the model to include the effect of temperature change on different model parameters, including the Nernst voltage, oxygen concentration, activation over potential,

water concentration, and resistance of the cell membrane. A new modular structure was also proposed for the FC to solve the problem caused by a drastic change in FC voltage. This guarantees MPPT and torque ripple reduction simultaneously. The simulation results demonstrated a fast dynamic model response and, therefore, it can be suitable for a variable speed drive.

Nomenclature

V_{FC}	Cell voltage	ρ_M	Specific resistance of membrane
E	Nernst voltage (reversible voltage)	l	Thickness of the membrane
V_{act}	Activation voltage	A	Useful area of membrane
V_{con}	Concentration voltage	ψ	Water content of the membrane
V_{ohm}	Ohmic voltage	B	Coefficient
ΔG	Gibbs free energy change	J	Current density
F	Faraday's constant	$J_{\max}$	Maximum current density
ΔS	Standard mole entropy change	T_{ic}	Coefficient
T	Working temperature	T_{rt}	Coefficient
T_{ref}	Reference temperature	T_{it}	Coefficient
R	Gaseous constant	$\bar{v}_s$	Stator voltage
P_{H_2}	Effective partial pressure of hydrogen	R_s	Stator resistance
P_{O_2}	Effective partial pressure of oxygen	$\bar{i}_s$	Stator current
K_{H2}	Hydrogen valve constant	$\bar{\psi}_s$	Stator flux
τ_{H2}	Hydrogen time constant	R_r	Rotor resistance
$q_{H_2}^{in}$	Hydrogen inlet flow rate	$\bar{i}_r$	Rotor current
K_r	Constant value	$\bar{\psi}_r$	Rotor flux
I_{FC}	Fuel cell current	ω_r	Rotor angular speed
K_{O2}	Oxygen valve constant	L_s	Stator inductance
τ_{O2}	Oxygen time constant	L_m	Magnetizing inductance
$q_{O_2}^{in}$	Oxygen inlet flow rate	L_r	Rotor inductance
V_a	Volume of the cell anode channels	S_{ABC}	State of inverter switches
V_C	Volume of the cell cathode channels	T_e	Electrical torque
ζ_i	Model coefficients	P	Pole pairs number
C_{O_2}	Effective oxygen concentration	S_r	Torque increment slope
R_m	Membrane resistance	S_f	Torque reduction slope
R_c	Resistances of electrodes and plates	T_l	Load torque

References

[1] L. Palma, P.N. Enjeti, "A modular fuel cell, modular DC-DC converter concept for high performance and enhanced reliability", IEEE Transactions on Power Electronics, Vol. 24, pp. 1437–1443, 2009.

[2] C.N. Maxoulis, D.N. Tsinoglou, G.C. Koltsakis, "Modeling of automotive fuel cell operation in driving cycles", Energy Conversion and Management, Vol. 45, pp. 559–573, 2004.

[3] C. Bernay, M. Marchand, M. Cassir, "Prospects of different fuel cell technologies for vehicle applications", Journal of Power Sources, Vol. 108, pp. 139–152, 2002.

[4] F.Z. Peng, M. Shen, K. Holland, "Application of z-source inverter for traction drive of fuel cell—battery hybrid electric vehicles", IEEE Transactions on Power Electronics, Vol. 22, pp. 1054–1061, 2007.

[5] T. Yalcinoz, M.S. Alam, "Dynamic modeling and simulation of air-breathing proton exchange membrane fuel cell", Journal of Power Sources, Vol. 182, pp. 168–174, 2008.

[6] M. Guarnieri, V.D. Noto, F. Moro, "A dynamic circuit model of a small direct methanol fuel cell for portable electronic devices", IEEE Transactions on Industrial Electronics, Vol. 57, pp. 1865–1873, 2010.

[7] R. O'Hayre, S.W. Cha, W. Colella, F.B. Prinz, Fuel Cell Fundamentals, New York, Wiley, 2009.

[8] S. Yerramalla, A. Davari, A. Feliachi, T. Biswas, "Modeling and simulation of the dynamic behavior of a polymer electrolyte membrane fuel cell", Journal of Power Sources, Vol. 124, pp. 104–113, 2003.

[9] S. Busquet, C.E. Hubert, J. Labbe, D. Mayer, R. Metkemeijer, "A new approach to empirical electrical modeling of a fuel cell, an electrolyser or a regenerative fuel cell", Journal of Power Sources, Vol. 134, pp. 41–48, 2004.

[10] D. Yu, S. Yuvarajan, "Electronic circuit model for proton exchange membrane fuel cells", Journal of Power Sources, Vol. 142, pp. 23 –242, 2005.

[11] W. Friede, S. Rael, B. Davat, "Mathematical model and characterization of the transient behavior of a PEM fuel cell", IEEE Transactions on Power Electronics, Vol. 19, pp. 1234–1241, 2004.

[12] A. Gebregergis, P. Pillay, "Implementation of fuel cell emulation on DSP and dSPACE controllers in the design of power electronic converters", IEEE Transactions on Industry Applications, Vol. 46, pp. 285–294, 2010.

[13] F. Grasser, A. Rufer, "A fully analytical PEM fuel cell system model for control applications", IEEE Transactions on Industry Applications, Vol. 43, pp. 1499–1506, 2007.

[14] H. Lorenz, K.E. Noreikat, T. Klaiber, W. Fleck, J. Sonntag, G. Hornburg, A. Gaulhofer, "Method and device for vehicle fuel cell dynamic power control", US Patent No. 5646852, 1997.

[15] F.L. Chen, H.S. Chu, C.Y. Soong, W.M. Yan, "Effective schemes to control the dynamic behavior of the water transport in the membrane of PEM fuel cell", Journal of Power Sources, Vol. 140, pp. 243–249, 2005.

[16] J. Faiz, S.H. Hosseini, M. Ghaneei, A. Keyhani, A. Proca, "Direct torque control of induction motor for electric propulsion systems", Electric Power System Research, Vol. 51, pp. 95–101, 1999.

[17] J. Faiz, M.B.B. Sharifian, "Comparison of different switching patterns in direct torque control technique of induction motors", Electric Power Systems Research, Vol. 60, pp. 63–75, 2001.

[18] T. Geyer, G. Papafotiou, M. Morari, "Model predictive direct torque control - Part I: Concept, algorithm and analysis", IEEE Transactions on Industrial Electronics, Vol. 56, pp. 1894–1905, 2009.

[19] J. Jia, Q. Li, Y. Wang, Y.T. Cham, M. Han, "Modeling and dynamic characteristic simulation of a proton exchange membrane fuel cell", IEEE Transactions on Energy Conversion, Vol. 24, pp. 283–291, 2009.

[20] A. Beicha, "Modeling and simulation of proton exchange membrane fuel cell systems", Journal of Power Sources, Vol. 205, pp. 335–339, 2012.

[21] M.T. Outeiro, R. Chibante, A.S. Carvalho, A.T. de Almeida, "A parameter optimized model of a proton exchange membrane fuel cell including temperature effects", Journal of Power Sources, Vol. 185, pp. 952–960, 2008.

[22] J.M. Corrêa, F.A. Farret, L.N. Canha, M.G. Simões, "An electrochemical-based fuel-cell model suitable for electrical engineering automation approach", IEEE Transactions on Industrial Electronics, Vol. 51, pp. 1103–1112, 2004.

[23] M. Uzunoglu, M.S. Alam, "Dynamic modeling, design, and simulation of a combined PEM fuel cell and ultracapacitor system for stand-alone residential applications", IEEE Transactions on Energy Conversion, Vol. 21, pp. 767–775, 2006.

[24] Y. Zhan, H. Wang, J. Zhu, "Modeling and control of hybrid UPS system with backup PEM fuel cell/battery", International Journal of Electrical Power and Energy Systems, Vol. 43, pp. 1322–1331, 2012.

[25] T. Bjažić, Z. Ban, M. Milanovič, "Modeling of current mode controlled boost converter supplied by fuel cell suitable for controller design purposes", Journal of Power Sources, Vol. 198, pp. 203–217, 2012.

[26] M.Y. El-Sharkh, A. Rahman, M.S. Alam, P.C. Byrne, A.A. Sakla, T. Thomas, "A dynamic model for a stand-alone PEM fuel cell power plant for residential applications", Journal of Power Sources, Vol. 138, pp. 199–204, 2004.

[27] D. Prasad, B.P. Panigrahi, S.S. Gupta, "Digital simulation and hardware implementation of a simple scheme for direct torque control of induction motor", Journal of Energy Conversion and Management, Vol. 49, pp. 687–697, 2008.

[28] T. Riad, B. Hocine, M. Salima, "New direct torque neuro-fuzzy control based SVM-three level inverter-fed induction motor", International Journal of Control, Automation, and Systems, Vol. 8, pp. 425–432, 2010.